nature cell biology

BCOR regulates mesenchymal stem cell function by epigenetic mechanisms

Zhipeng Fan[1], Takayoshi Yamaza[2], Janice S. Lee[3], Jinhua Yu[1], Songlin Wang[4], Guoping Fan[5], Songtao Shi[2] and Cun-Yu Wang[1,6]

The BCL-6 co-repressor (BCOR) represses gene transcription by interacting with BCL-6 (refs 1, 2). *BCOR* mutation is responsible for oculo-facio-cardio-dental (OFCD) syndrome, which is characterized by canine teeth with extremely long roots, congenital cataracts, craniofacial defects and congenital heart disease[3–5]. Here we show that *BCOR* mutation increased the osteo-dentinogenic potential of mesenchymal stem cells (MSCs) isolated from a patient with OFCD, providing a molecular explanation for abnormal root growth. *AP-2*α was identified as a repressive target of BCOR, and *BCOR* mutation resulted in abnormal activation of *AP-2*α. Gain- and loss-of-function assays suggest that *AP-2*α is a key factor that mediates the increased osteo-dentinogenic capacity of MSCs. Moreover, we found that BCOR maintained tissue homeostasis and gene silencing through epigenetic mechanisms. *BCOR* mutation increased histone H3K4 and H3K36 methylation in MSCs, thereby reactivating transcription of silenced target genes. By studying a rare human genetic disease, we have unravelled an epigenetic mechanism for control of human adult stem cell function.

OFCD is a rare genetic disorder characterized by teeth with extremely long roots (radiculomegaly), and craniofacial, ocular and cardiac abnormalities[3–7]. OFCD is inherited in an X-linked dominant pattern in heterozygous females. Males with OFCD cannot survive because of embryonic lethality. Frequent ocular anomalies include congenital cataracts and microphthalmia. Facial deformities include long narrow face, high nasal bridge and cleft palate. Congenital cardiac abnormalities include septal defects and mitral valve defects. Among the many dental defects reported in OFCD patients, enlargement of the roots of canine teeth is the most consistent and typical finding[3–7]. The roots consist mainly of dentin, a bone-like mineralized tissue that anchors the tooth in alveolar bone. After tooth eruption, root formation is well-synchronized with alveolar bone growth and stops growing at certain ages[8–11]. By contrast, in OFCD patients, the roots of mandibular incisors and canines can grow continuously until they reach the lower border of the mandible; the roots of maxillary incisors and canines can extend to the cortical plate of the orbit. Thus, canine radiculomegaly has been considered to be an important sign in the diagnosis of OFCD[3–7].

Genetic studies have found that mutations in *BCOR* are responsible for OFCD syndrome[3]. Mutations in *BCOR*, usually truncation and frameshift mutations, result in premature termination of the protein with deletion of the carboxy-terminal domain[3–5]. BCOR was originally identified as a co-repressor of the transcription repressor BCL-6 (ref. 1). Chromosomal translocations of BCL-6 are common genomic alterations in non-Hodgkin's B-cell lymphomas[12]. BCOR has been found to interact with histone deacetylase (HDAC), demethylase and H2A ubiquitin ligase, suggesting that BCOR might mediate repression through chromatin modification[1,13,14]. In mice, *Bcor* has been found to be expressed in the tooth primordium, eye, neural tube and branchial arches, which correlate with tissues affected in OFCD patients[15]. Genetic studies, through deleting *Bcor* in embryonic stem cells, suggest that *Bcor* has an important role in early mouse embryonic development[16].

MSCs were originally isolated from bone marrow and are multipotent as they can differentiate into a variety of cell types including osteoblasts, chondrocytes, myocytes and adipocytes. Increasing evidence indicates that MSCs are also present in non-bone marrow tissues[17–21]. Recently, a new population of MSCs has been isolated from dental and craniofacial tissues on the basis of their stem cell properties[11,22,23]. These cells are multipotent, osteo-dentinogenic and capable of self-renewal. When transplanted into immunocompromised mice, they generated bone/dentin-like mineralized tissue and were capable of repairing dental and craniofacial defects[11,24]. Characterization of MSCs from the root apical papilla strongly suggests that these cells are responsible for root dentin formation and root growth. As patients with OFCD have enlarged and continuously growing roots, *BCOR* mutation could have an intrinsic effect on the proliferation and function of MSCs from the root apical papilla. To test our hypothesis, we isolated MSCs from the root apical papilla of an OFCD patient and examined their stem cell

[1]Lab of Molecular Signaling, Division of Oral Biology and Medicine, UCLA School of Dentistry, Los Angeles, California 90095, USA. [2]Center for Craniofacial Molecular Biology, University of Southern California School of Dentistry, Los Angeles, California 90033, USA. [3]Department of Oral and Maxillofacial Surgery, University of San Francisco, San Francisco 94143, CA, USA. [4]Molecular Laboratory for Gene Therapy and Tooth Regeneration, Capital Medical University School of Stomatology, Beijing 100050, China. [5]Department of Human Genetics, UCLA School of Medicine, Los Angeles, California 90095, USA.
[6]Correspondence should be addressed to C.-Y.W. (e-mail: cwang@dentistry.ucla.edu)

Received 27 February 2009; accepted 22 April 2009; published online 5 July 2009; DOI: 10.1038/ncb1913

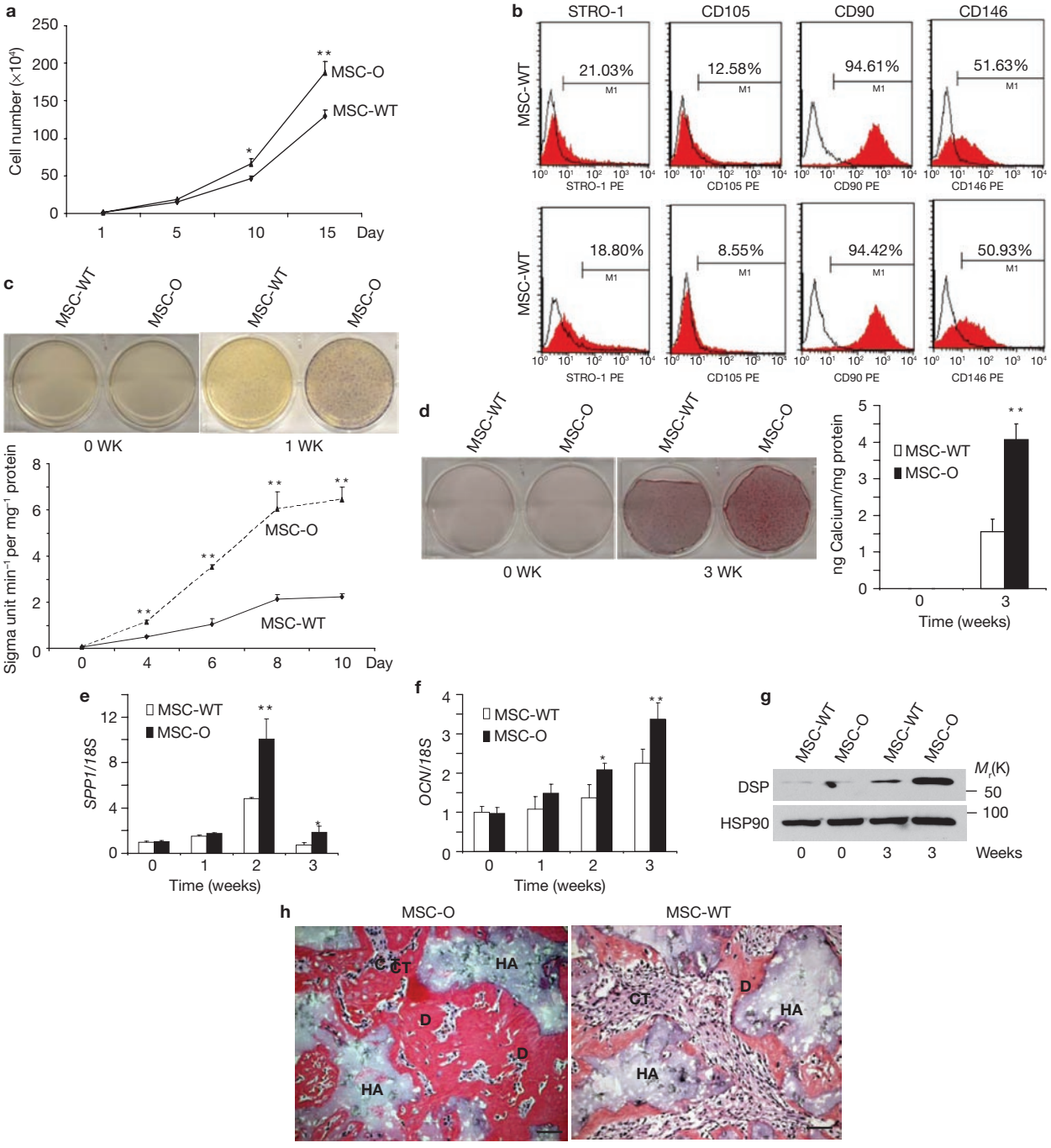

Figure 1 *BCOR* mutation results in enhanced osteo-dentinogenic potential of MSCs from a patient with OFCD. (**a**) *BCOR* mutation promoted MSC proliferation. Values are mean ± s.d. for triplicate samples of MSC-O and MSC-WT cells in a representative experiment (*P <0.05; **P < 0.01, Student's *t*-test). (**b**) Flow cytometry showed that *BCOR* mutation did not affect expression of stem cell surface markers. Cells were sorted on a FACSCalibur flow cytometer and analysed using Cell Quest software (BD Bioscience). (**c**) *BCOR* mutation resulted in enhanced ALP activity in MSCs. Values in the lower panel are mean ± s.d. for triplicate samples from a representative experiment shown in the upper panel (**P <0.01, Student's *t*-test). (**d**) *BCOR* mutation resulted in enhanced mineralization in MSC-O cells. Values in the right panel are mean ± s.d. for triplicate samples from a representative experiment shown in the left panel (**P <0.01, Student's *t*-test). (**e**, **f**) *BCOR* mutation resulted in enhanced expression of *SPP1* (**e**) and *OCN* (**f**) in MSC-O cells. Expression of both *SPP1* and *OCN* was examined by real-time RT–PCR. Values are mean ± s.d. for triplicate samples from a representative experiment (**P <0.01, Student's *t*-test). (**g**) *BCOR* mutation resulted in enhanced DSP expression in MSC-O cells. DSP expression was examined by western blot analysis. HSP90 was used as an internal control. Uncropped images of the blots are shown in the Supplementary Information, Fig. S6. (**h**) *BCOR* mutation resulted in enhanced mineralized tissue formation *in vivo*. MSC-O and MSC-WT cells were transplanted into SCID mice for 8 weeks. D, bone/dentin-like tissues; HA, hydroxyapatite tricalcium carrier; CT, connective tissues. Scale bar, 100 μm.

properties. *BCOR* mutation did not affect expression of stem cell markers, but resulted in enhanced osteo-dentinogenic potential of MSCs by inducing AP-2α. Mechanistically, we found that *BCOR* mutation increased histone H3K4 and H3K36 methylation, and reduced binding

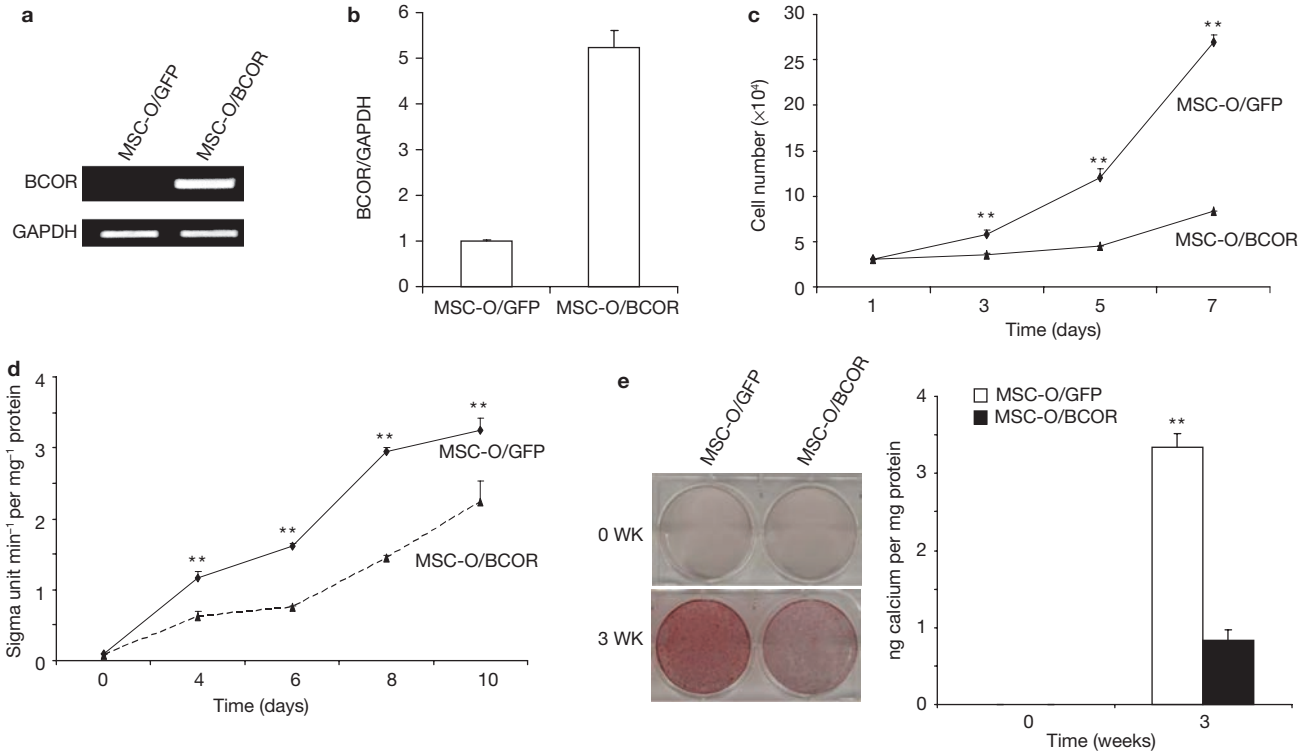

Figure 2 Restoration of wild-type *BCOR* in MSC-O cells inhibited cell differentiation and proliferation. (**a**) Overexpression of *BCOR* in MSC-O cells. Wild-type *Flag–BCOR* was ectopically expressed in MSC-O cells as determined by RT–PCR using specific primers for *Flag–BCOR*. *GAPDH* was used as an internal control. (**b**) *BCOR* overexpression was determined by real-time RT–PCR. Real-time RT–PCR was performed using primers that detected endogenous *BCOR* and ectopic *Flag–BCOR*. Values are mean ± s.d. for triplicate samples. (**c**) Overexpression of *BCOR* inhibited MSC-O cell proliferation. Values are mean ± s.d. for triplicate samples from a representative experiment (**P <0.01, Student's t-test). (**d**) Overexpression of BCOR inhibited ALP activity in MSC-O cells. Values are mean ± s.d. for triplicate samples from a representative experiment (**P <0.01, Student's t-test). (**e**) Overexpression of *BCOR* inhibited mineralization in MSC-O cells. Values are mean ± s.d. for triplicate samples from a representative experiment (**P <0.01, Student's t-test).

of BCL-6 to the *AP-2α* promoter, thereby resulting in a loss of BCL–6/BCOR repressive function. Our results provide a molecular explanation for the abnormal root growth seen in OFCD syndrome.

MSCs were isolated from the apical papilla of an OFCD patient with radiculomegaly undergoing surgical removal of the root apex. This patient had a single nucleotide deletion, c.2613delC, resulting in a frameshift mutation with a premature stop codon, p.F871Lfs8X[4]. As with many of the mutations found in other patients with OFCD, this frameshift mutation led to deletion of the BCOR carboxy terminus (approximately 800 amino acid deletion). MSCs isolated from the OFCD patient (MSC-O) proliferated at a faster rate *in vitro* than wild-type MSCs isolated from a healthy individual (MSC-WT; Fig. 1a; Supplementary Information, Fig. S1a). Notably, expression levels of *BCOR* mRNA in MSC-WT and MSC-O cells were similar (Supplementary Information, Fig. S1b, c). Increased proliferation could not fully account for the phenotype of OFCD, as radiculomegaly indicated that the root was heavily mineralized. Thus, we further examined whether *BCOR* mutation intrinsically affected MSC function. FACS profiling showed that MSC-O cells expressed stem cell markers of MSCs that were similar to those of MSC-WT cells (Fig. 1b)[11,20,21]. Root dentin is a specialized mineralized tissue similar to bone[8,10,11]. As root formation is abnormal in patients with OFCD, we tested whether MSC-O cells had increased osteo-dentinogenic potential. MSC-O and MSC-WT cells were treated with differentiation-inducing medium containing dexamethasone, ascorbic acid and β-glycerophosphate, as described previously[11]. To minimize the effect of cell growth on differentiation, MSC-O and MSC-WT cells were plated under confluent conditions. Soon after induction, alkaline phosphatase (ALP) activity, an early marker for osteo-dentinogenic differentiation, was more strongly induced in MSC-O cells, compared with MSC-WT cells (Fig. 1c). Three weeks after induction, Alizarin Red staining revealed that calcium deposition or mineralization was also significantly higher in MSC-O cells than in MSC-WT cells (Fig. 1d). Consistently, real-time RT–PCR showed that genes, including *OCN* and *SPP1*, which encode extracellular matrix proteins of bone and dentin, were more strongly induced in MSC-O cells, compared with MSC-WT cells (Fig. 1e, f). Dental sialoprotein (DSP) is an extracellular matrix protein highly expressed in dentin, compared with other tissues[8,10,25]. We found that induction of DSP was significantly higher in MSC-O cells than in MSC-WT cells (Fig. 1g). *In vivo* transplantation experiments also demonstrated that MSC-O cells generated more bone/dentin-like mineralized tissue, compared with MSC-WT cells (Fig. 1h).

As OFCD is an X-linked dominant syndrome in heterozygous females, the initial MSC-O cells from the patient could be a mixed population expressing wild-type or mutant *BCOR* mRNA because of X-inactivation. Thus, it is important to determine whether enhanced osteo-dentinogenic differentiation in passaged MSC-O cells is mainly due to cells expressing mutant *BCOR* mRNA. Total

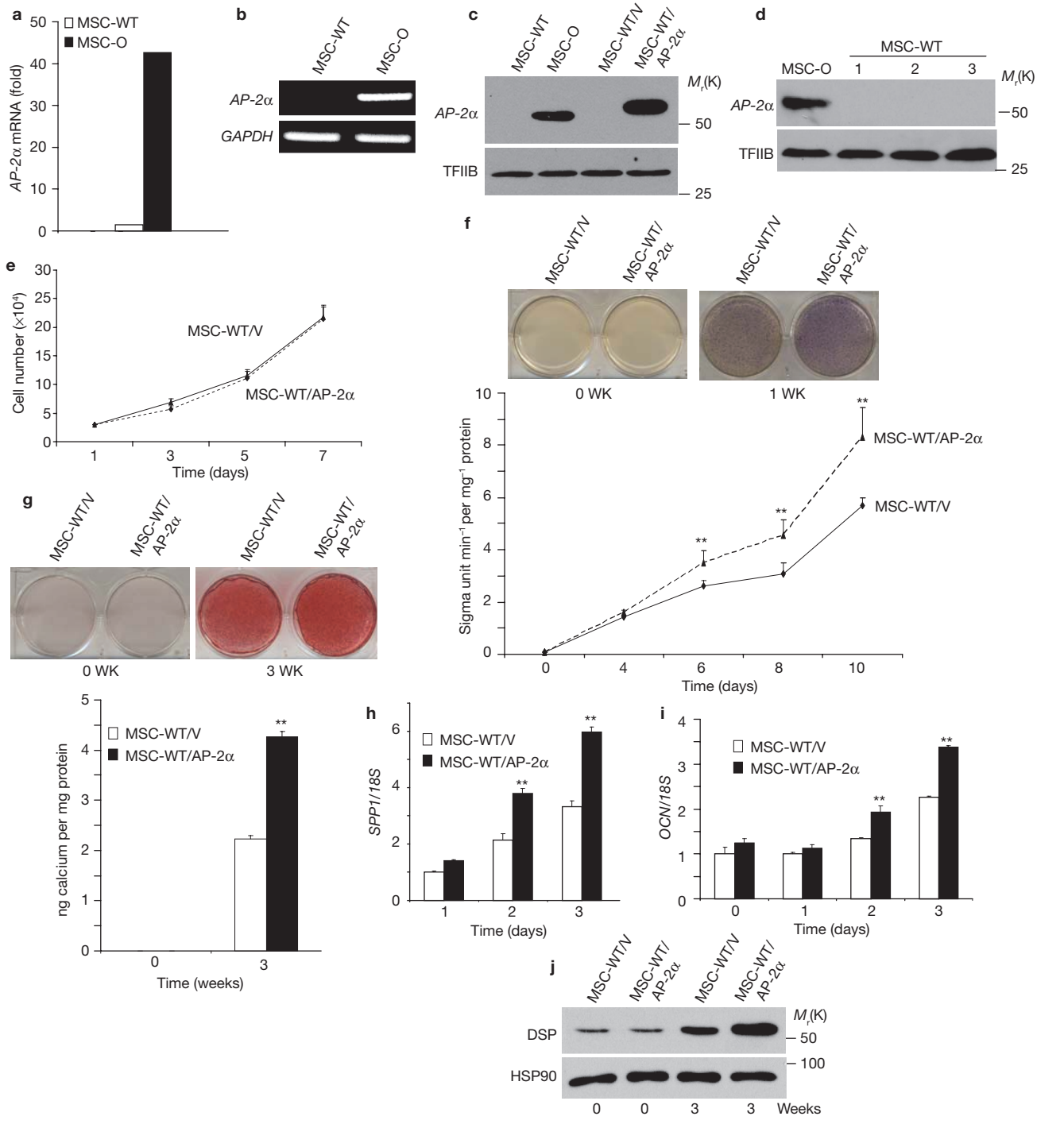

Figure 3 *BCOR* mutation increases AP-2α expression in MSC-O cells. (**a**) Gene expression profile revealed that *AP-2α* was highly expressed in MSC-O cells. (**b**) Expression of *AP-2α* was greater in MSC-O cells than in MSC-WT cells. *AP-2α* expression was determined by RT–PCR. *GAPDH* was used as an internal control. (**c**) Western blot analysis showed that AP-2α expression was greater in MSC-O cells than in MSC-WT cells. Uncropped images of the blots are shown in Supplementary Information, Fig, S6. (**d**) AP-2α was not detected in normal MSC-WT cells from three different healthy individuals. Uncropped images of the blots are shown in Supplementary Information, Fig. S6. (**e**) Overexpression of AP-2α did not affect MSC proliferation. Values are mean ± s.d. for triplicate samples from a representative experiment. (**f**) Overexpression of AP-2α increased ALP activity in MSC cells. Values in the lower panel are mean ± s.d. for triplicate samples from a representative experiment shown in the upper panel (**P <0.01, Student's t-test). (**g**) Overexpression of AP-2α increased mineralization in MSCs. Values in the lower panel are mean ± s.d. for triplicate samples from a representative experiment shown in the upper panel (**P <0.01,Student's t-test). (**h**, **i**) Overexpression of AP-2α enhanced *SPP1* (**h**) and *OCN* (**i**) expression in MSCs. *SPP1* and *OCN* expression was determined by real-time RT–PCR. Values are mean ± s.d for triplicate samples from a representative experiment (**P <0.01, Student's t-test). (**j**) Overexpression of AP-2α enhanced DSP expression in MSC cells. DSP expression was determined by western blot analysis. HSP90 was used as an internal control. Uncropped images of the blots are shown in Supplementary Information, Fig, S6.

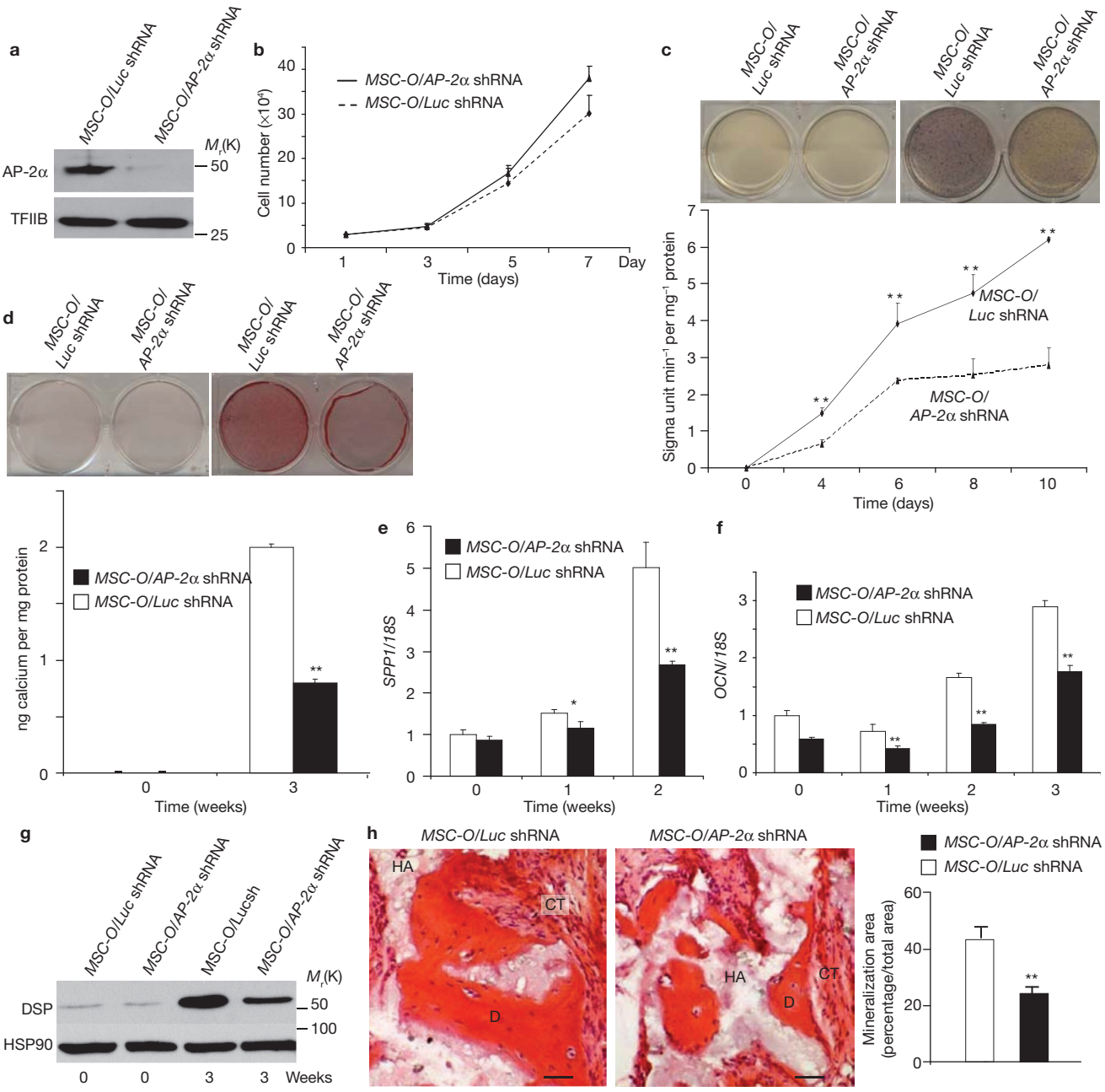

Figure 4 AP-2α is a key mediator of the enhanced osteo-dentinogenic potential of MSCs by *BCOR* mutation. (**a**) Knockdown of *AP-2α* in MSC-O cells. *MSC-O/Luc* shRNA, MSC-O cells expressing *luciferase* shRNA; *MSC-O/AP-2α* shRNA, MSC-O cells expressing *AP-2α* shRNA. Uncropped images of the blots are shown in the Supplementary Information, Fig, S6. (**b**) Depletion of AP-2α in MSC-O cells did not significantly affect cell proliferation. Values are mean ± s.d. for triplicate samples from a representative experiment. (**c**) Knockdown of *AP-2α* reduced ALP activity in MSC-O cells. Values in the lower panel are mean ± s.d. for triplicate samples from a representative experiment shown in the upper panel (**P <0.01, Student's *t*-test). (**d**) Knockdown of *AP-2α* reduced mineralization in MSC-O cells. Values in the lower panel are mean ± s.d. for triplicate samples from a representative experiment shown in the lower panel (**P <0.01, Student's *t*-test). (**e**, **f**) Real-time RT–PCR showed that knockdown of *AP-2α* decreased expression of *SPP1* (**e**) and *OCN* (**f**) in MSC-O cells. Values are mean ± s.d. for triplicate samples from a representative experiment (*P <0.05; **P <0.01, Student's *t*-test). (**g**) Knockdown of *AP-2α* decreased DSP expression in MSC-O cells. Uncropped images of the blots are shown in the Supplementary Information, Fig, S6. (**h**) Knockdown of *AP-2α* reduced mineralized tissue formation *in vivo*. Both *MSC-O/AP-2α* shRNA and *MSC-O/Luc* shRNA cells were transplanted subcutaneously into the dorsal surface of 10-week old immunocompromised beige mice. Values are mean ± s.d., $n = 5$ (**P <0.01, Student's *t*-test). Scale bar, 100 μm.

RNA from MSC-O cells was extracted and RT–RCR was performed using specific primers that were from different exons and spanned the mutation site of *BCOR*. The PCR products were subcloned into a TA clone vector and sequenced. We found that most of the clones (52 out of 60) expressed mutant *BCOR* (Supplementary Information, Fig. S1d), suggesting that the mutant cells outgrew the wild-type cells in expanded MSC-O cell cultures. To further confirm our results, we also used small hairpin RNA (shRNA) to knock down *BCOR* in MSC-WT cells. Knockdown of *BCOR* expression significantly enhanced osteo-dentinogenic differentiation of MSC-WT cells

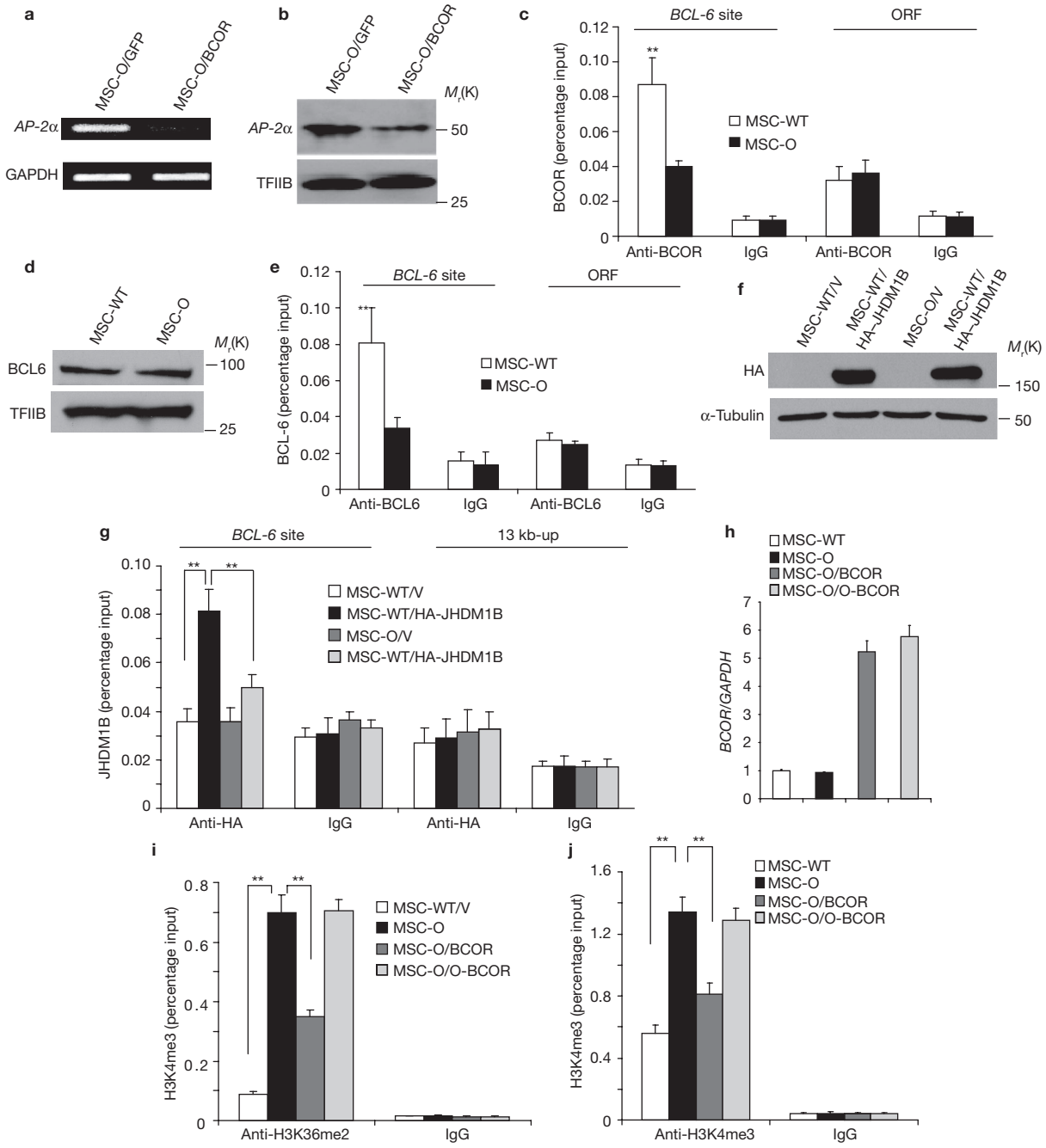

Figure 5 BCOR represses AP-2α transcription by epigenetic mechanisms. (**a**) Overexpression of *BCOR* suppressed *AP-2α* expression in MSC-O cells as determined by RT–PCR. (**b**) Overexpression of BCOR suppressed AP-2α expression in MSC-O cells as determined by western blot analysis. Uncropped images of the blots are shown in the Supplementary Information, Fig, S6. (**c**) BCOR was not detected in the *AP-2α* promoter in MSC-O cells. Chromatin and DNA complexes were immunoprecipitated with anti-BCOR antibodies. $^{**}P<0.01$, Student's *t*-test. (**d**) BCL-6 expression in MSC-WT and MSC-O cells was examined by western blot analysis. Uncropped images of the blots are shown in the Supplementary Information, Fig, S6. (**e**) *BCOR* mutation impaired BCL-6 binding to the *AP-2α* promoter. ChIP assays were performed with anti-BCL-6 antibodies or control IgG. $^{**}P<0.01$, Student's *t*-test. (**f**) Overexpression of JHDM1B in MSC-WT and MSC-O cells. Cells were transduced with retroviruses expressing HA–JHDM1B or control empty vector. Uncropped images of the blots are shown in the Supplementary Information, Fig, S6. (**g**) *BCOR* mutation failed to recruit JHDM1B to the *AP-2α* promoter. ChIP assays were performed with anti-HA antibodies or control IgG. $^{**}P<0.01$, Student's *t*-test. (**h**) Overexpression of *BCOR* or *O-BCOR* in MSC-O cells. (**i**) *BCOR* mutation resulted in increased histone H3K36 methylation in the *AP-2α* promoter. ChIP assays were performed with anti-H3K36me2 antibodies or control IgG. $^{**}P<0.01$, Student's *t*-test. (**j**) *BCOR* mutation resulted in increased histone H3K4 methylation in the *AP-2α* promoter. ChIP assays were performed with anti-H3K4me3 antibodies or control IgG. $^{**}P<0.01$, Student's *t*-test. Values are mean ± s.d. for triplicate samples from a representative experiment in **c**, **e**, **g**–**j**.

(Supplementary Information, Fig. S2). Moreover, knockdown of *BCOR* in MSCs isolated from the dental pulp, also known as dental pulp stem cells (DPSCs)[26], markedly enhanced osteo-dentinogenic differentiation (Supplementary Information, Fig. S3).

To determine whether the enhanced osteo-dentinogenic potential associated with MSC-O cells was directly due to *BCOR* mutation, we tested whether the restoration of wild-type *BCOR* (isoform C) in MSC-O could inhibit the osteo-dentinogenic potential of MSC-O cells. To rule out clonal variation, MSC-O cells were transduced with retroviruses expressing *Flag–BCOR* and control vector. Using specific primers to detect *Flag–BCOR*, RT–PCR confirmed that wild-type *BCOR* was stably expressed in MSC-O (MSC-O/BCOR) cells, but not in control cells (MSC-O/GFP) (Fig. 2a). Real-time RT–PCR showed a 5-fold increase in *BCOR* mRNA expression in MSC-O/BCOR cells, compared with MSC-O/GFP cells (Fig. 2b), using primers which detect both endogenous *BCOR* and ectopic *Flag–BCOR*. Overexpression of wild-type *BCOR* significantly inhibited proliferation of MSC-O cells (Fig. 2c). Restoration of wild-type BCOR in MSC-O cells strongly inhibited ALP activity when differentiation was induced (Fig. 2d). Consistently, mineralization was markedly inhibited in MSC-O/BCOR cells, compared with MSC-O/GFP cells, as determined by Alizarin Red staining (Fig. 2e).

Our studies suggest that *BCOR* mutation has intrinsic effects on the differentiation capacity of MSCs. However, because *BCOR* mutation increases cell proliferation, the enhancement of osteo-dentinogenic potential of MSCs might be an indirect effect. To resolve this crucial issue, we performed gene expression profiling to identify the BCOR target genes that might be associated with osteo-dentinogenic potential using Affymetrix Human Genome U133 Plus 2.0 Array. Together with this information, gain- and loss-of-function experiments would help to determine whether BCOR-regulated target genes were crucial for enhanced osteo-dentinogenic potentials, thereby providing direct evidence to verify the functional role of *BCOR* mutation in osteo-dentinogenic capacity. Importantly, microarray revealed that *AP-2α* was the second highest differentially expressed gene in MSC-O cells, compared with MSC-WT cells (Fig. 3a). Other genes that are highly expressed in MSC-O cells (>5-fold) relative to MSC-WT cells are listed in Supplementary Information, Table S1. Previously, genetic studies showed that *AP-2α* was associated with craniofacial development and that *AP-2α* knockout caused craniofacial and skeletal defects[27,28]. RT–PCR confirmed that *AP-2α* was strongly expressed in MSC-O cells, but not in MSC-WT cells (Fig. 3b). Consistently, western blot analysis showed that AP-2α was highly expressed in MSC-O cells, but was only barely detectable in MSC-WT cells (Fig. 3c). Furthermore, we found that AP-2α was not expressed in MSCs from three different healthy individuals, indicating that the difference was unlikely to be caused by individual variation (Fig. 3d).

To determine whether AP-2α is a key mediator for enhanced osteo-dentinogenic potential resulting from *BCOR* mutation, we first tested whether overexpression of AP-2α would potentiate the differentiation capacity of MSC-WT cells. To avoid clonal variation, MSC-WT cells were transduced with retroviruses expressing *Flag–AP-2α* or control vector. Western blot analysis confirmed that AP-2α was expressed (Fig. 3c). Overexpression of AP-2α did not affect MSC proliferation (Fig. 3e). We found that overexpression of AP-2α significantly enhanced ALP activity and mineralization on induction (Fig. 3f, g). Real-time RT–PCR and western blot analysis also revealed that overexpression of AP-2α enhanced expression of *OCN*, *SPP1* and DSP (Fig. 3h–j).

To further confirm that AP-2α was responsible for the enhanced osteo-dentinogenic potential of MSCs, we used shRNA to knockdown *AP-2α* expression in MSC-O cells. Western blot analysis confirmed that approximately 90% of AP-2α in MSC-O cells were knocked down by retroviruses expressing *AP-2α* shRNA (Fig. 4a). Knockdown of *AP-2α* did not significantly change cell proliferation (Fig. 4b), but it significantly reduced ALP activity and mineralization in MSC-O cells (Fig. 4c, d). Consistently, knockdown of *AP-2α* decreased expression of *OCN*, *SPP1* and DSP (Fig. 4e–g). We transplanted MSC-O cells expressing *AP-2α* shRNA (MSC-O/*AP-2α* shRNA) and MSC-O expressing *luciferase* shRNA (MSC-O/*Luc* shRNA) into nude mice. Knockdown of *AP-2α* also significantly reduced bone/dentin-like tissue formation *in vivo* (Fig. 4h).

RT–PCR and western blot analysis showed that overexpression of BCOR suppressed AP-2α expression in MSC-O cells (Fig. 5a, b). Conversely, knockdown of *BCOR* in MSC-WT cells increased *AP-2α* expression (Supplementary Information, Fig. S2b). These results further confirm that BCOR controls AP-2α expression. We then examined whether BCOR was associated with the *AP-2α* promoter in MSC cells. A BCL-6-binding site (TTTAGGAA), which is located 1,439 bp upstream of the transcription start site, was found on the *AP-2α* promoter. Chromatin co-immunoprecipitation (ChIP) assays revealed that BCOR was present at the BCL-6-binding site of *AP-2α* in MSC-WT cells, but not in MSC-O cells (Fig. 5c). Notably, anti-BCOR antibodies could not recognize the mutant BCOR proteins in MSC-O cells. As a negative control, BCOR was not detected in a region located in the open reading frame (ORF) of *AP-2α*. Interestingly, although BCL-6 was expressed at similar levels (Fig. 5d), its binding to the *AP-2α* promoter was reduced in MSC-O cells, compared with MSC-WT cells (Fig. 5e). Recent studies have shown that the BCOR complex contains polycomb group proteins and JHDM1B/FBXL10 demethylase[13,14]. Although the functional role of these molecules in the BCOR complex is not clear, their findings suggest that BCOR might use an epigenetic mechanism to direct gene silencing. Abnormal histone methylation resulting from *BCOR* mutation might affect BCL-6 binding to the *AP-2α* promoter. JHDM1B is a histone demethylase that has been shown to demethylate trimethylated Lys 4 or dimethylated Lys 36 on histone 3 (H3K4me3 or H3K36me2)[29,30]. In general, methylation at H3K4 and H3K36 is associated with transcriptional activation[31,32]. As the BCOR carboxy terminus is required to interact with these molecules, we hypothesized that *BCOR* mutation in OFCD might impair recruitment of JHDM1B to chromatin. However, despite our repeated efforts, anti-JHDM1B antibodies that were available were not effective in our ChIP assays. To overcome this problem, we used retroviruses to express HA–JHDM1B in MSC-WT and MSC-O cells (Fig. 5f) and performed ChIP assays using anti-HA antibodies. HA–JHDM1B on the *AP-2α* promoter in MSC-WT cells was significantly higher than that in MSC-O cells (Fig. 5g). Moreover, we directly examined whether *BCOR* mutation affected H3K4 and H3K36 methylation of the *AP-2α* promoter in MSCs. ChIP assays revealed that H3K36me2 on the *AP-2α* promoter in MSC-O cells was 7-fold higher than in MSC-WT cells (Fig. 5i). H3K4me3 on the *AP-2α* promoter in MSC-O cells was also significantly increased (Fig. 5j). To further confirm our results, we overexpressed wild-type and OFCD mutant forms of *BCOR* (*O-BCOR*) in MSC-O cells (Fig. 5h). ChIP assays showed that restoration of wild-type *BCOR* significantly reduced H3K4me3 and H3K36me2 in MSC-O cells (Fig. 5i, j). By contrast, overexpression of O-BCOR had no effect on H3K4 or H3K36 methylation in MSC-O cells. Of note, a recent study showed that JHDM1B is an H3K36me2-specific demethylase. H3K4me3 changes might be indirect[33]. To determine whether the BCOR–JHDM1B complex had a role in the inhibition of MSC function, we used shRNA to knock down *JHDM1B*

(Supplementary Information, Fig. S4a) in MSC-WT cells. Depletion of *JHDM1B* resulted in the induction of *AP-2α* expression (Supplementary Information, Fig. S4b). and enhanced osteo-dentinogenic differentiation of MSC-WT cells (Supplementary Information, Fig. S4c–f). Finally, as the BCOR complex is associated with ubiquitylation of histone H2A, we performed ChIP assays to determine whether *BCOR* mutation affects ubiquitylation of H2A. ChIP assays revealed that ubiquitylation of H2A was significantly reduced in MSC-O cells, compared with MSC-WT cells (Supplementary Information, Fig. S5).

Our studies provide a possible explanation for dental and craniofacial defects in patients with OFCD. We have shown that *BCOR* mutation led to the upregulation of AP-2α in MSCs and promoted osteo-dentinogenesis. Mechanistically, *BCOR* has a crucial role in development and maintenance of homeostasis through epigenetic modification of histone methylation. Under normal conditions, BCOR interacts with JHDM1B and represses gene transcription by inhibiting H3K4 and H3K36 methylation on the target gene promoter in MSCs. In patients with OFCD, the *BCOR* mutation fails to recruit JHDM1B to the target gene promoter, resulting in increased H3K4 and H3K36 methylation, and transcription activation of silenced gene in MSCs. Supporting this conclusion, depletion of JHDM1B in MSCs also induces AP-2α expression and enhances osteo-dentinogenic differentiation of MSCs. On the basis of our microarray results, the BCOR complex might repress a large number of genes in MSCs. In addition to *AP-2α*, it is possible that other genes could also have a role in dental and craniofacial defects in patients with OFCD. For example, *PAX3*, which is associated with craniofacial development, is also activated in MSC-O cells. In addition to craniofacial defects, cataracts are the most frequent ocular phenotype of OFCD patients[3,4]. Interestingly, transgenic mice overexpressing AP-2α developed cataracts[34], further supporting the notion that AP-2α has a role in the pathogenesis of OFCD. MSCs are also involved in cardiac development and formation. In future studies, it will be interesting to examine how *BCOR* mutation affects heart development and whether AP-2α plays a role in congenial heart defects associated with OFCD patients. In summary, by studying a rare human genetic disease, we identified the BCOR complex as a negative regulator of osteo-dentiogenic capacity of MSCs. □

METHODS

Methods and any associated references are available in the online version of the paper at http://www.nature.com/naturecellbiology/

Note: Supplementary Information is available on the Nature Cell Biology website.

ACKNOWLEDGEMENTS

This work was supported by the National Institute of Dental and Craniofacial Research Grants (R01DE1016513 and R01DE017684) to C.Y.W. (R21DE017632) and S.S., and the Shapiro Family Charitable Foundation. We thank Vivian Bardwell for reagents.

AUTHOR CONTRIBUTIONS

Z.F., T.Y. and J.Y. performed experiments and prepared figures; J.S.L. prepared samples and directed the experiments; G.F. and S.W. assisted with the genetic analysis; S.S. and C.Y.W. designed the experiments and analysed the data; C.Y.W. wrote the manuscript.

COMPETING INTERESTS STATEMENT

The authors declare that they have no competing financial interests.

Published online at http://www.nature.com/naturecellbiology/
Reprints and permissions information is available online at http://npg.nature.com/reprintsandpermissions/

1. Huynh, K. D., Fischle, W., Verdin, E. & Bardwell, V. J. BCoR, a novel co-repressor involved in BCL-6 repression. *Genes Dev.* **14,** 1810–1823 (2000).
2. Ghetu, A. F. *et al.* Structure of a BCOR co-repressor peptide in complex with the BCL-6 BTB domain dimer. *Mol. Cell* **29,** 384–391 (2008).
3. Ng, D. *et al.* Oculofaciocardiodental and Lenz microphthalmia syndromes result from distinct classes of mutations in *BCOR*. *Nature Genet.* **36,** 411–416 (2004).
4. Oberoi, S., Winder, A. E., Johnston, J., Vargervik, K. & Slavotinek, A. M. Case reports of oculofaciocardiodental syndrome with unusual dental findings. *Am. J. Med. Genet. A.* **136,** 275–277 (2005).
5. Horn, D. *et al.* Novel mutations in BCOR in three patients with oculo-facio-cardio-dental syndrome, but none in Lenz microphthalmia syndrome. *Eur. J. Hum. Genet.* **13,** 563–569 (2005).
6. Hedera, P. & Gorski, J. L. Oculo-facio-cardio-dental syndrome: skewed X chromosome inactivation in mother and daughter suggest X-linked dominant Inheritance. *Am. J. Med. Genet. A.* **123A**, 261–266 (2003).
7. Schulze, B. R., Horn, D., Kobelt, A., Tariverdian, G. & Stellzig, A. Rare dental abnormalities seen in oculo-facio-cardio-dental (OFCD) syndrome: three new cases and review of nine patients. *Am. J. Med. Genet.* **82,** 429–435 (1999).
8. Foster, B. L., Popowics, T. E., Fong, H. K. & Somerman, M. J. Advances in defining regulators of cementum development and periodontal regeneration. *Curr. Top. Dev. Biol.* **78,** 47–126 (2007).
9. Kim, J. W. & Simmer, J. P. Hereditary dentin defects. *J. Dent. Res.* **86,** 392–399 (2007).
10. MacDougall, M., Dong, J. & Acevedo, A. C. Molecular basis of human dentin diseases. *Am. J. Med. Genet. A.* **140,** 2536–2546 (2006).
11. Sonoyama, W. *et al.* Mesenchymal stem cell-mediated functional tooth regeneration in swine. *PLoS ONE* **1**, e79 (2006).
12. Ye, B. H. *et al.* Alterations of a zinc finger-encoding gene, BCL-6, in diffuse large-cell lymphoma. *Science* **262,** 747–750 (1993).
13. Gearhart, M. D., Corcoran, C. M., Wamstad, J. A. & Bardwell, V. J. Polycomb group and SCF ubiquitin ligases are found in a novel BCOR complex that is recruited to BCL6 targets. *Mol. Cell Biol.* **26,** 6880–6889 (2006).
14. Sanchez, C. *et al.* Proteomics analysis of Ring1B/Rnf2 interactors identifies a novel complex with the Fbxl10/Jhdm1B histone demethylase and the Bcl6 interacting corepressor. *Mol. Cell Proteomics* **6,** 820–834 (2007).
15. Wamstad, J. A. & Bardwell, V. J. Characterization of Bcor expression in mouse development. *Gene Expr. Patterns* **7,** 550–557 (2007).
16. Wamstad, J. A., Corcoran, C. M., Keating, A. M. & Bardwell, V. J. Role of the transcriptional corepressor Bcor in embryonic stem cell differentiation and early embryonic development. *PLoS ONE* **3**, e2814 (2008).
17. Jahagirdar, B. N. & Verfaillie, C. M. Multipotent adult progenitor cell and stem cell plasticity. *Stem Cell Rev.* **1,** 53–59 (2005).
18. Phinney, D. G. & Prockop, D. J. Concise review: mesenchymal stem/multipotent stromal cells: the state of transdifferentiation and modes of tissue repair—current views. *Stem Cells* **25,** 2896–2902 (2007).
19. Scaffidi, P. & Misteli, T. Lamin A-dependent misregulation of adult stem cells associated with accelerated ageing. *Nature Cell Biol.* **10,** 452–459 (2008).
20. Shi, S. *et al.* Bone formation by human postnatal bone marrow stromal stem cells is enhanced by telomerase expression. *Nature Biotechnol.* **20,** 587–591 (2002).
21. Shi, S. & Wang, C. Y. Bone marrow stromal stem cells for repairing the skeleton. *Biotechnol. Genet. Eng. Rev.* **21,** 133–143 (2004).
22. Seo, B. M. *et al.* Investigation of multipotent postnatal stem cells from human periodontal ligament. *Lancet* **364,** 149–155 (2004).
23. Arthur, A., Rychkov, G., Shi, S., Koblar, S. A. & Gronthos, S. Adult human dental pulp stem cells differentiate towards functionally active neurons under appropriate environmental cues. *Stem Cells* (2008).
24. Chang, J. *et al.* Noncanonical Wnt-4 signaling enhances bone regeneration of mesenchymal stem cells in craniofacial defects through activation of p38 MAPK. *J. Biol. Chem.* **282,** 30938–30948 (2007).
25. Butler, W. T., Brunn, J. C. & Qin, C. Dentin extracellular matrix (ECM) proteins: comparison to bone ECM and contribution to dynamics of dentinogenesis. *Connect. Tissue Res.* **44 Suppl 1,** 171–178 (2003).
26. Scheller, E. L., Chang, J. & Wang, C. Y. Wnt/β-catenin inhibits dental pulp stem cell differentiation. *J. Dent. Res.* **87,** 126–130 (2008).
27. Schorle, H., Meier, P., Buchert, M., Jaenisch, R. & Mitchell, P. J. Transcription factor AP-2 essential for cranial closure and craniofacial development. *Nature* **381,** 235–238 (1996).
28. Brewer, S., Feng, W., Huang, J., Sullivan, S. & Williams, T. Wnt1-Cre-mediated deletion of AP-2α causes multiple neural crest-related defects. *Dev. Biol.* **267,** 135–152 (2004).
29. Frescas, D., Guardavaccaro, D., Bassermann, F., Koyama-Nasu, R. & Pagano, M. JHDM1B/FBXL10 is a nucleolar protein that represses transcription of ribosomal RNA genes. *Nature* **450,** 309–313 (2007).
30. Tsukada, Y. *et al.* Histone demethylation by a family of JmjC domain-containing proteins. *Nature* **439,** 811–816 (2006).
31. Shi, Y. & Whetstine, J. R. Dynamic regulation of histone lysine methylation by demethylases. *Mol. Cell* **25,** 1–14 (2007).
32. Klose, R. J., Kallin, E. M. & Zhang, Y. JmjC-domain-containing proteins and histone demethylation. *Nature Rev. Genet.* **7,** 715–727 (2006).
33. He, J., Kallin, E. M., Tsukada, Y. & Zhang, Y. The H3K36 demethylase Jhdm1b/Kdm2b regulates cell proliferation and senescence through p15(Ink4b). *Nature Struct. Mol. Biol.* **15,** 1169–1175 (2008).
34. West-Mays, J. A., Coyle, B. M., Piatigorsky, J., Papagiotas, S. & Libby, D. Ectopic expression of AP-2α transcription factor in the lens disrupts fiber cell differentiation. *Dev. Biol.* **245,** 13–27 (2002).

DOI: 10.1038/ncb1913

METHODS

Cell cultures and viral infection. Tissues were obtained under approved guidelines set by the University of California San Francisco Institutional Review Board with informed patient consent. Cells were grown in a humidified 5% CO_2 incubator at 37 °C in Dulbecco's modified alpha modified Eagle's medium (Invitrogen) supplemented with 15% fetal bovine serum (FBS; Invitrogen). MSC-O cells were derived from a single patient with OFCD and used for all analysis. MSC-WT cells were obtained from multiple healthy subjects. Full-length *AP-2α* and *JHDM1B* mRNAs from MSC-O cells were amplified by RT–PCR and then subcloned into pQCXIP retroviral vector (BD Biosciences). pCLMFG Flag–BCOR/C IRES eGFP plasmids were provided by Vivian Bardwell at the University of Minnesota. Viral packaging was prepared as described previously[35]. For viral infection, MSCs were plated overnight and then infected with retroviruses in the presence of polybrene (6 μg ml^{-1}, Sigma-Aldrich) for 6 h. The target sequences for shRNA were: *AP-2α*, 5′-TCCAGGAAGATCTTTAAGA-3′; *BCOR*, 5′-GATGGCTTCAGTGCTATAT-3′; *JHDM1B*, 5′-GAGTCAAGACGTAGAATAA-3′ and *luciferase*, 5′-GTGCGTTGCTAGTACCAAC-3′. The shRNA was subcloned into a pSIREN retroviral vector (BD Bioscience) and retrovirus packaging was performed as described previously[35].

Western blot analysis. Cells were lysed in RIPA buffer (10 mM Tris-HCL, 1 mM EDTA, 1% sodium dodecyl sulfate (SDS), 1% Nonidet P-40, 1: 100 proteinase inhibitor cocktail, 50 mM β-glycerophosphate, 50 mM sodium fluoride). The samples were separated on a 10% SDS polyacrylamide gel and transferred to PVDF membrane by a semi-dry transfer apparatus (Bio-Rad). The membranes were blotted with 5% milk for 2 h and then incubated with primary antibodies overnight. The immunocomplexes were incubated with horseradish peroxidase-conjugated anti-rabbit or anti-mouse IgG (Promega) and visualized with SuperSignal reagents (Pierce). Primary antibodies were purchased from the following commercial sources: monoclonal antibodies against AP-2α (1:200), polyclonal antibodies against HSP90 and TFIIB (1:1,000; Santa Cruz); monoclonal antibodies against ubiquitylated H2A (1:500; Millipore); polyclonal antibodies against H3K4me3 (1:500; Abcam) and H3K36me2 (1:500; Upstate); polyclonal antibodies against dentin sialoprotein (DSP; 1:1,000; NIDCR/NIH, USA); polyclonal anti-BCL-6 antibodies (1:1,000; Cell Signaling); monoclonal antibodies against α-tubulin (1:100,000; Sigma-Aldrich).

ALP and Alizarin Red staining. MSCs were grown in mineralization-inducing medium containing 100 μM ascorbic acid, 2 mM β-glycerophosphate and 10 nM dexamethasone. For ALP staining, after induction, cells were fixed with 70% ethanol and incubated with a solution of 0.25% naphthol AS-BI phosphate and 0.75% Fast Blue BB dissolved in 0.1 M Tris buffer (pH 9.3). ALP activity assay was performed with an ALP kit according to the manufacturer's protocol (Sigma-Aldrich) and normalized on the basis of protein concentrations. To assess mineralization, cells were induced for 2–3 weeks, fixed with 70% ethanol and stained with 2% Alizarin Red (Sigma-Aldrich). To quantitatively determine calcium mineral density, Alizarin Red was destained with 10% cetylpyridinium chloride in 10 mM sodium phosphate for 30 min at room temperature. The concentration was determined by absorbance measurement at 562 nm on a multiplate reader using a standard calcium curve prepared in the same solution. The final calcium levels in each group were normalized with the total protein concentrations prepared from duplicate plates[20].

Reverse transcriptase-polymerase chain reaction (RT–PCR) and real-time RT–PCR. Total RNA was isolated from MSCs using Trizol reagents (Invitrogen). The primers used were: *AP-2α*, forward, 5′-CTCTCACCACCCGAGTGTCT-3′ and reverse, 5′- GAGGTTGAAGTGGGTCAAGC-3′; *BCOR*, forward, CTCAGGAGACCACCCAGTC-3′ and reverse, 5′-CCCTGAGCCACAGATACTTG-3′; *glyceraldehyde-3-phosphate dehydrogenase* (*GAPDH*) , forward, 5′-GATCATCAGCAATGCCTCCT-3′ and reverse, 5′-ACCTGGTGCTCAGTGTAGCC-3′. For RT–PCR, 2-μg aliquots of RNAs were synthesized using random hexamers and reverse transcriptase according to the manufacturer's protocol (Invitrogen).

Real-time PCR reactions were performed using the QuantiTect SYBR Green PCR kit (Qiagen) and Icycler iQ Multi-color real-time PCR detection system. Primers used were: *SPP1*, forward, 5′-ATGATGGCCGAGGTGATAGT-3′ and reverse, 5′-ACCATTCAACTCCTCGCTTT-3′; *OCN* , forward, 5′-AGCAAAGGTGCAGCCTTTGT-3′ and reverse, 5′-GCGCCTGGGTCTCTTCACT-3′; *JHDM1B*, forward, 5′-ACTTGACCATACCAATGGCGGT-3′; and reverse, 5′-AAGCTGGTCAGGATTGCCAGAA-3′; *BCOR*, forward, 5′-CATAGTGCTTGTGGAACTCCG-3′ and reverse, 5′-GGACACAGCTCTCCTGTTGC-3′; *AP-2α*, forward, 5′-CTGCAGGGAGACGTAAAGC and reverse, 5′-GGCTAGGTGGACAGCTTCTC-3′; *18S rRNA*, forward, 5′-CGGCTACCACATCCAAGGAA-3′ and reverse, 5′-GCTGGAATTACCGCGGCT-3′; *GAPDH*, forward, 5′CGGCTACCACATCCAAGGAA-3′ and reverse, 5′-AGCCACATCGCTCAGACACC-3′.

Human affymetrix microarray. Total RNAs were extracted from MSC-WT and MSC-O cells with Trizol reagents and cleaned with an RNeasy kit (Qiagen). Total RNA (5-μg aliquots) from each sample were transcribed to double-stranded complementary DNA (cDNA) using SuperScript II RT (Invitrogen) with an oligo-dT primer and then used to generate single-stranded RNAs. The biotin-labelled RNAs were fragmented and hybridized with an Affymetrix Human Genome U133 Plus 2.0 Array. The arrays were scanned with the GeneArray scanner (Affymetrix). The one-step Tukey's Biweight Estimate was used to calculate signal intensity. Affymetrix Microarray Suite (MAS) 5.0 was used for data analysis[35].

ChIP assays. The assay was performed using a ChIP assay kit (Upstate) according to the manufacturer's protocol. Polyclonal antibodies against BCOR were provided by Vivian Bardwell at the University of Minnesota. Cells were incubated with 5 mM dimethyl 3,3′ dithiobispropionimidate-HCl (Pierce) solution for 10 min at room temperature before formaldehyde treatment. For each ChIP reaction, 2×10^6 cells were used. All resulting precipitated DNA samples were quantified with real-time PCR. Data were expressed as the percentage of input DNA. The BCL-6 binding site was detected in 1,439 bp upstream of the *AP-2α* transcription start site. The surrounding region of the binding site was used for amplification. The primer sequences were: BCL-6-binding region of the *AP-2α* promoter, forward, 5′GTGAGGGAATGCTCCAATCT-3′ and reverse, 5′-CCTTTGATTCATCTGGGCTT; *ORF*, forward, 5′- CCTCGAAGTACAAGGTCACG-3′ and reverse, 5′-GACACTCGGGTGGTGAGAG-3′; 13kb up of *AP-2α*, forward, 5′-CCGCCCTGTCTCTGGTACTTTC-3′ and reverse, 5′-AGCACCTTCTATACAGCATTCG-3′.

Transplantation in nude mice. Approximately 4.0×10^6 of cells were mixed with 40 mg of hydroxyapatite/tricalcium phosphate (HA/TCP) ceramic particles (Zimmer) and then transplanted subcutaneously into the dorsal surface of 10-week-old immunocompromised beige mice as described previously[11,24]. These procedures were performed in accordance with the approved University of Southern California animal protocol (USC#10874). Eight weeks after transplantation, the transplants were collected, fixed with 10% formalin, decalcified with buffered 10% EDTA (pH 8.0), and then embedded in paraffin. Sections were deparaffinized, hydrated and stained with haemotoxylin and eosin.

Accession numbers. The accession number for the microarray data is GSE15214.

35. Park, B. K. *et al.* NF-κB in breast cancer cells promotes osteolytic bone metastasis by inducing osteoclastogenesis via GM-CSF. *Nature Med.* **13,** 62–69 (2007).

nature cell biology

DOI: 10.1038/ncb1913

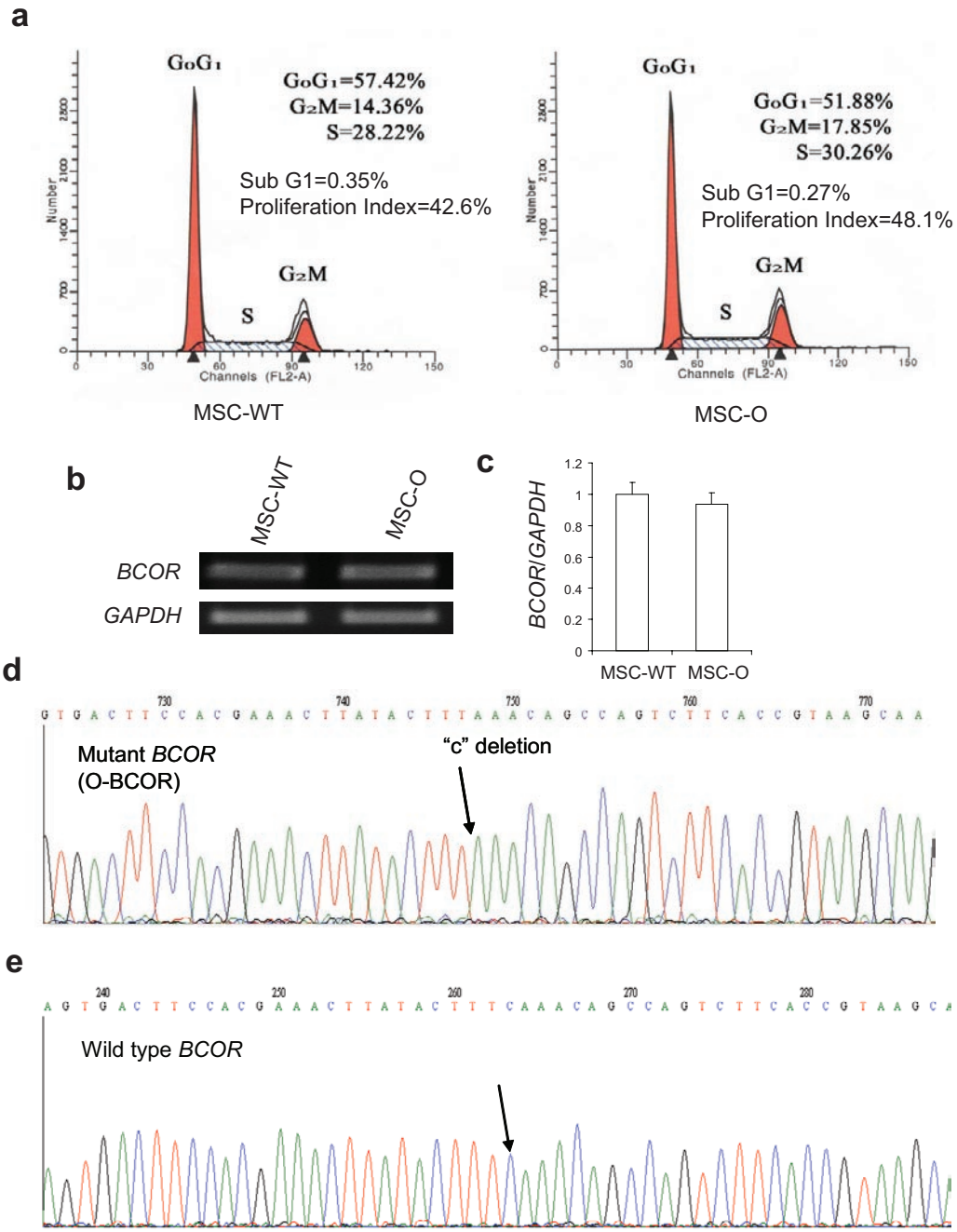

Figure S1 Mutant cells outgrow wild type cells in expanded MSC-O cell culture. (**a**) BCOR mutation increases MSC proliferation. Cell sorting and analysis were performed on a FACSVantage SE (Beckton Dickson, Mountain View, CA). The proliferation index (PI) in MSC-O cells is significantly higher than in MSC-WT cells (*P<0.05). (**b**) The expression level of *BCOR* mRNA in both MSC-WT and MSC-O cells was determined by RT-PCR. (**c**) The expression level of *BCOR* mRNA in both MSC-WT and MSC-O cells was determined by Real-time RT-PCR. The error bars represent s.d. (n = 3). (**d**) A single nucleotide "c" deletion in MSC-O cells. A total of 60 clones were picked up for sequencing. 52 of 60 (86.7) clones contained a single nucleotide "c" deletion in *BCOR*. (**e**) Sequencing of wild type *BCOR*.

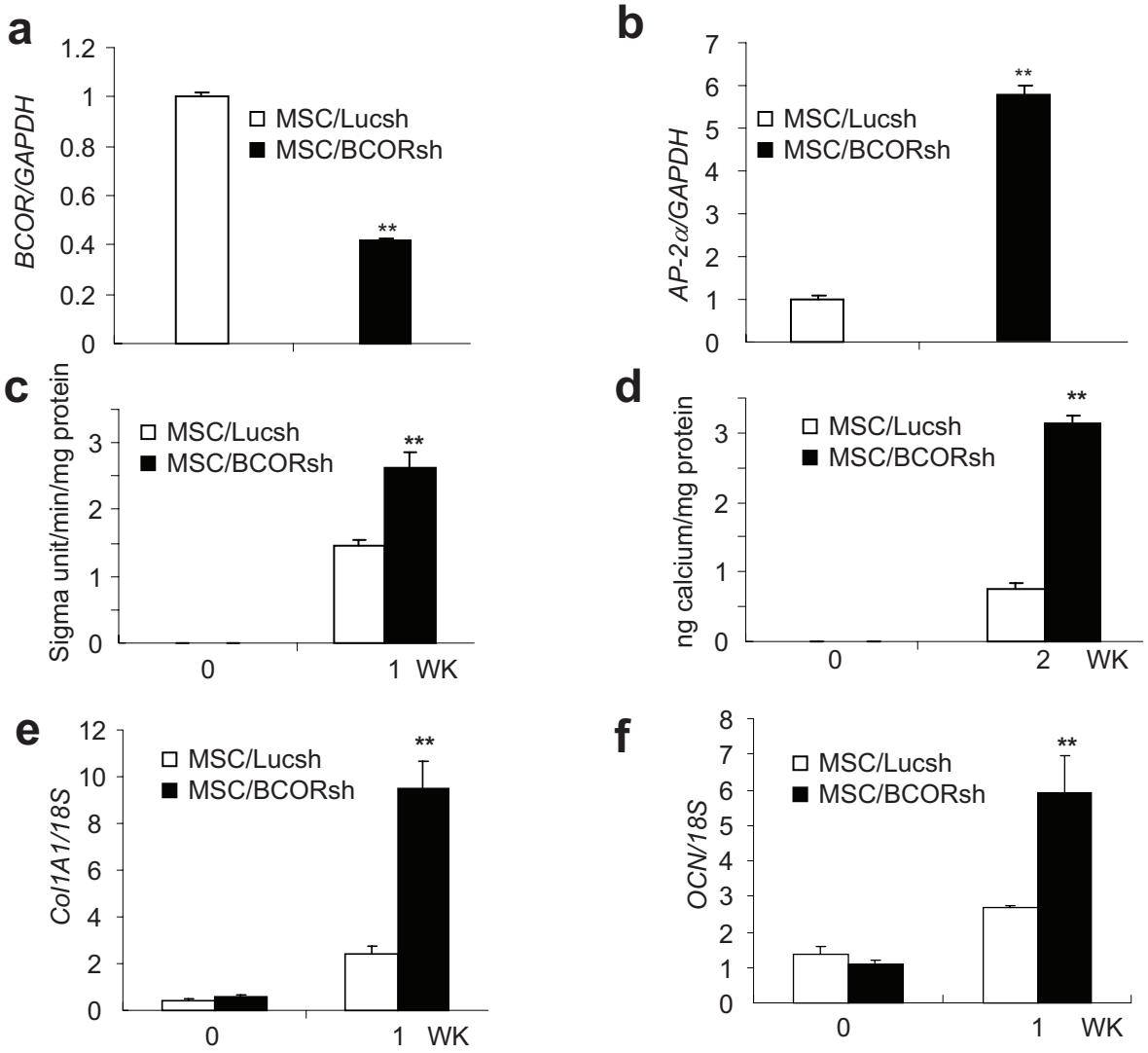

Figure S2 The knock-down of BCOR in MSC-WT cells enhances MSC differentiation. (**a**) *BCOR* in MSC-WT cells was knocked down by shRNA. shRNA was targeted for all isoforms of BCOR. (**b**) The knock-down of *BCOR* in MSC-WT cells induced *AP-2α* expression as determined by Real-time RT-PCR. (**c**), The knock-down of BCOR induced ALP activity in MSC-WT cells. (**d**) The knock-down of BCOR induced mineralization in MSC-WT cells. (**e**) The knock-down of BCOR increased *COL1A1* expression in MSC-WT cells as determined by Real-time RT-PCR. (**f**) The knock-down of BCOR increased *OCN* expression in MSC-O cells by Real-time RT-PCR. **P<0.01. Values (**a**-**f**) are mean ± s.d for triplicate samples from a representative experiment. Student's t test was performed to determine statistical significance. **P < 0.01.

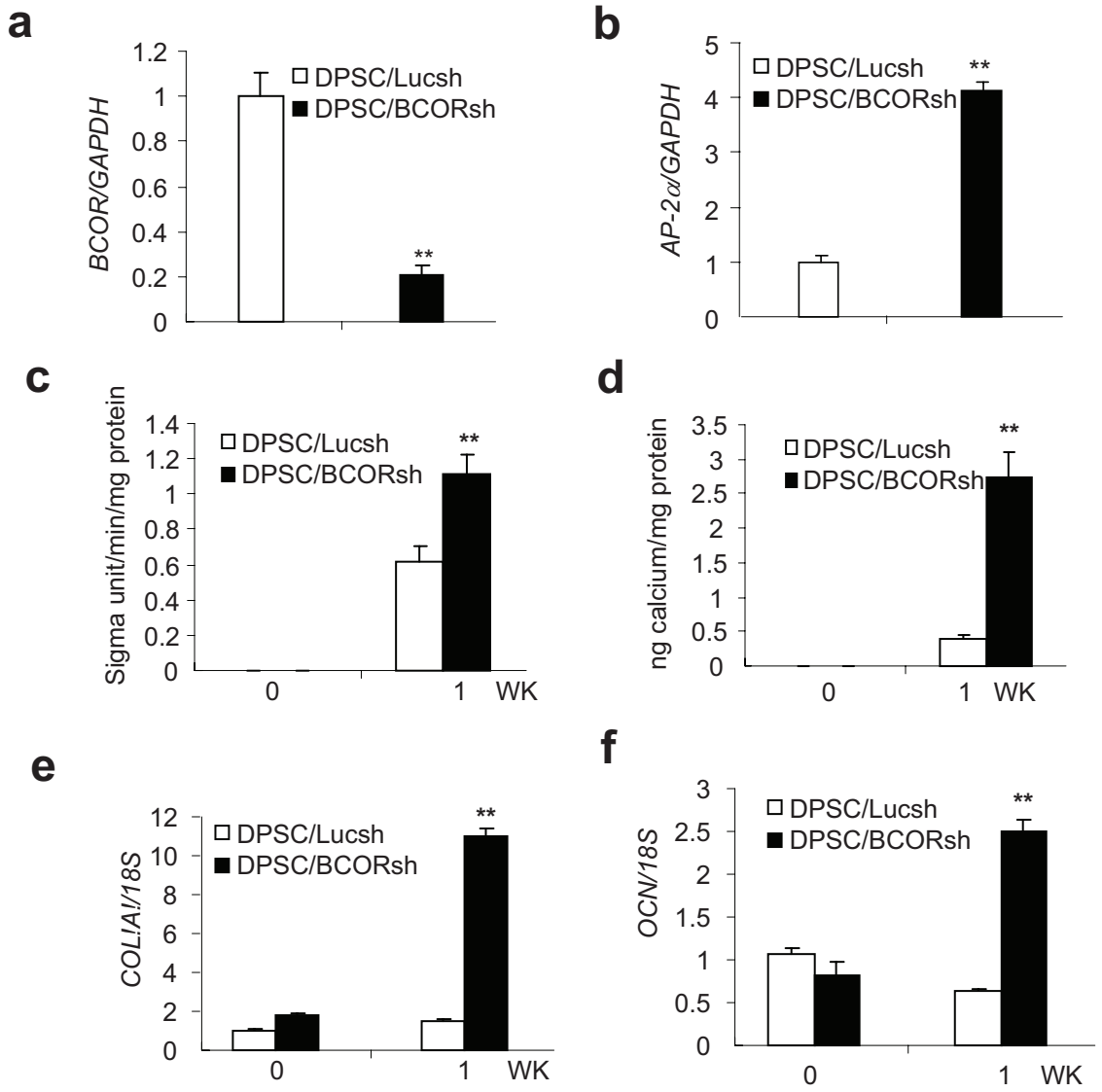

Figure S3 The knock-down of BCOR in MSC from the dental pulp (DSPC) enhances osteogenic/dentinogenic differentiation. (**a**) *BCOR* in DSPCs was knocked down by shRNA. (**b**) The knock-down of BCOR in DSPCs induced *AP-2α* expression as determined by Real-time RT-PCR. (**c**) The knock-down of BCOR induced ALP activity in DSPCs. (**d**) The knock-down of BCOR induced mineralization in DSPCs. (**e**) The knock-down of BCOR increased *COL1A1* expression in DSPCs as determined by Real-time RT-PCR. (**f**) The knock-down of BCOR increased *OCN* expression in DSPCs as determined by Real-time RT-PCR. Values (**a**-**f**) are mean ± s.d for triplicate samples from a representative experiment. Student's t test was performed to determine statistical significance. **P < 0.01.

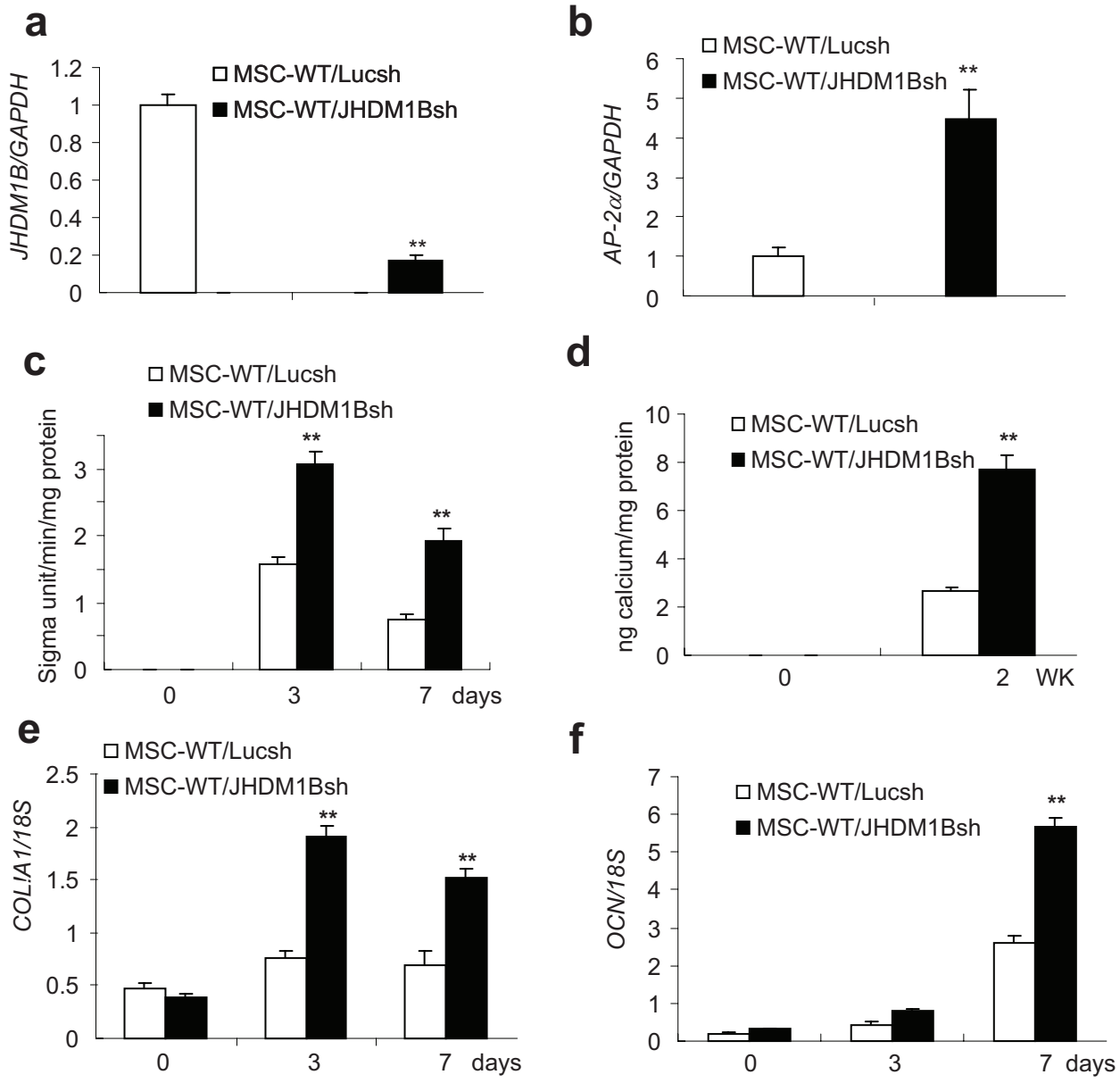

Figure S4 The knock-down of JHDM1B in MSC-WT cells enhances MSC differentiation. (**a**) *JHDM1B* in MSC-WT cells was knocked down by shRNA as determined by Real-time RT-PCR. (**b**) The knock-down of *JHDM1B* in MSC-WT cells induced *AP-2α* expression as determined by Real-time RT-PCR. (**c**) The knock-down of *JHDM1B* enhanced ALP activity in MSC-WT cells. (**d**) The knock-down of *JHDM1B* enhanced mineralization in MSC-WT cells. (**e**) The knock-down of *JHDM1B* increased *COL1A1* expression in MSC-WT cells as determined by Real-time RT-PCR. (**f**) The knock-down of *JHDM1B* increased *OCN* expression in MSC-O cells as determined by Real-time RT-PCR. Values (**a**-**f**) are mean ± s.d for triplicate samples from a representative experiment. Student's t test was performed to determine statistical significance. **P < 0.01.

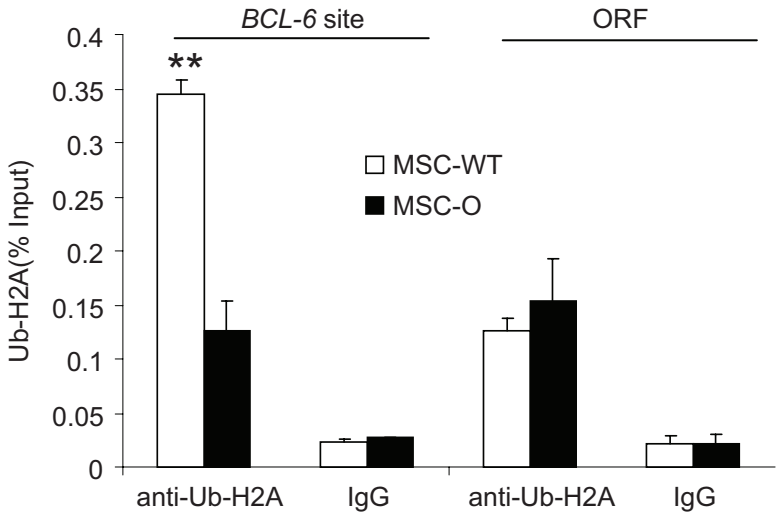

Figure S5 The *BCOR* mutation affects H2A ubiquitination. ChIP assays were performed with anti-Ub-H2A antibodies or control IgG. The error bars represent s.d. (n=3). **P < 0.01.

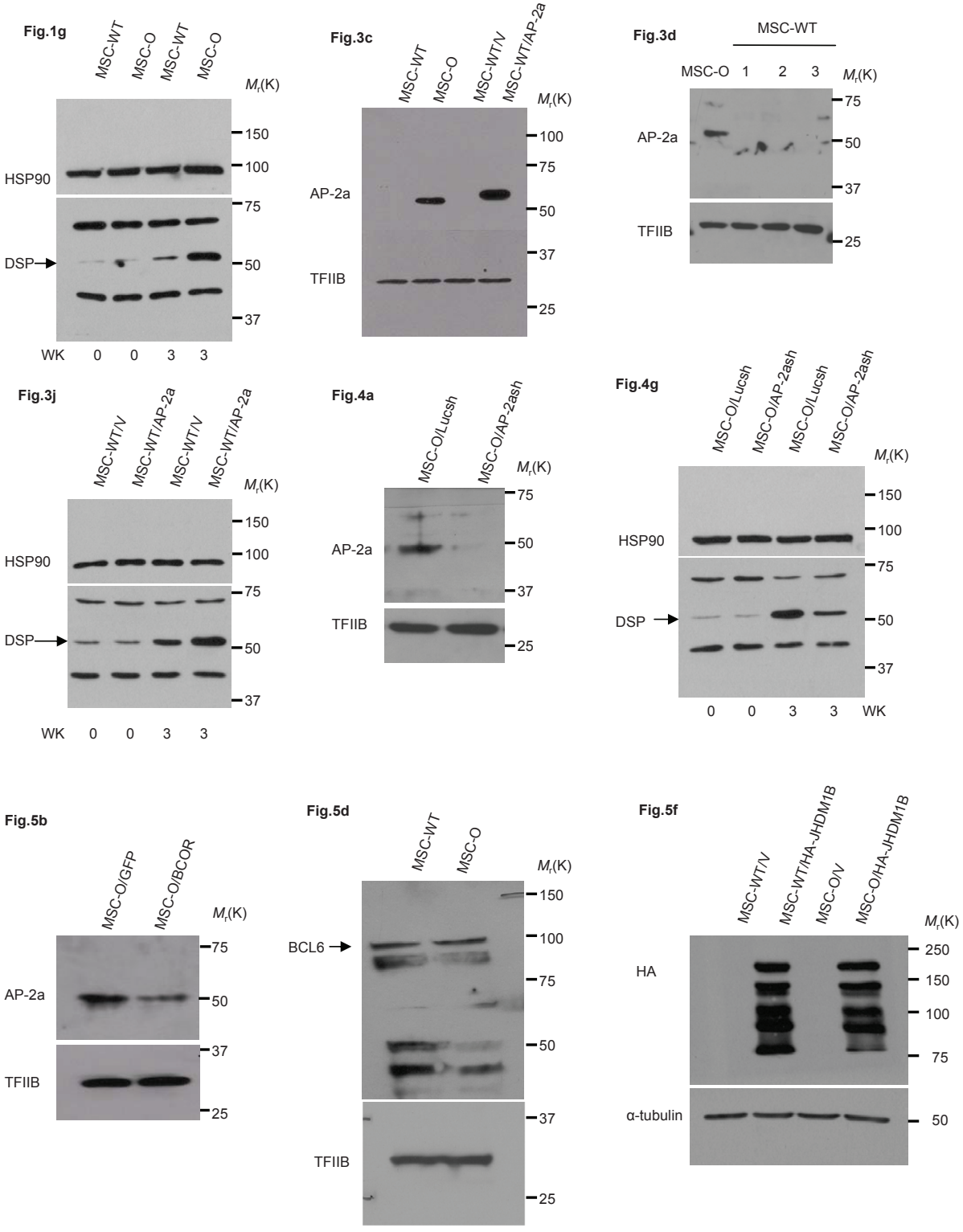

Figure S6 The full-scans of gel presented in the paper are shown with molecular weight markers.